K. P. Walker and E. M. Jordan†*

Biaxial Constitutive Modelling and Testing of a Single Crystal Superalloy at Elevated Temperatures

REFERENCE Walker, K. P. and Jordan, E. H., **Biaxial constitutive modelling and testing of a single crystal superalloy at elevated temperatures**, *Biaxial and Multiaxial Fatigue*, EGF 3 (Edited by M. W. Brown and K. J. Miller), 1989, Mechanical Engineering Publications, London, pp. 145–170.

ABSTRACT A viscoplastic constitutive model for single crystal superalloys is developed from crystallographic slip theory. The model is applied to the tension and torsion deformation behaviour of the single crystal superalloy PWA 1480 at 871°C (1600°F). Both octahedral and cube slip behaviour are needed to model the deformation behaviour of single crystal superalloys at elevated temperature.

Introduction

The trend towards improved engine efficiency and durability places increasing demands on materials that operate in the hot sections of gas turbine engines. These demands are being met by new coatings and materials such as single crystal and directionally solidified nickel-base superalloys which have greater creep/fatigue resistance at elevated temperatures and reduced susceptibility to grain boundary creep, corrosion, and oxidation than conventionally cast alloys (1).

In order to fully utilize the advantages of these new materials, new constitutive models, life prediction methods, and 3-dimensional structural analysis tools must be developed to provide efficient and effective designs. The new constitutive models and life prediction methods must account both for the strong directional behaviour of these new anisotropic alloys and for the time-dependence or viscoplastic behaviour of the materials during high temperature operation.

This paper represents initial work carried out as part of a research program aimed at the development of constitutive equations to describe the elevated temperature stress–strain behaviour of single crystal and directionally solidified turbine blade alloys. The program involves both the development of suitable constitutive models and verification of the models through elevated temperature tension–torsion testing.

A viscoplastic constitutive model for the single crystal alloy is derived from postulated material behaviour on individual crystallographic slip systems. The

* Engineering Science Software, Inc., Smithfield, RI, USA.
† University of Connecticut, Storrs, CT, USA.

behaviour of the entire single crystal is then arrived at by summing up the slip on all the operative crystallographic slip systems. This type of formulation has a number of important advantages, including the prediction of deformation orientation dependence and the ability to directly represent the constitutive behaviour in terms which metallurgists use in describing the micromechanisms.

Metallurgical background

The cast single crystal nickel-base superalloy PWA 1480 has been under development at Pratt & Whitney for nearly 11 years and has been successfully tested as a blade alloy in both commercial and military engines. Other single crystal alloys such as the AIResearch alloy MAR–M247, the General Electric alloy René–N4 and the Canon–Muskegon alloy CMSX–2 are also being used in gas turbine engines. These alloys were developed in order to eliminate the grain boundaries which are present in conventionally cast equiaxed polycrystalline superalloys, and which are susceptible to grain boundary corrosion, cracking, and creep deformation. In alloy PWA 1480 (also known as alloy 454) the normal grain boundary strengthening elements (hafnium, carbon, boron, and zirconium) have been deleted. These elements are also melting point depressants and without them the single crystal alloy PWA 1480 has an incipient melt temperature above 1280°C (2370°F). This allows nearly complete γ' solutioning during heat treatment and a reduction in dendritic segregation. The absence of grain boundaries, the opportunity for full solution heat treatment, and the reduced dendritic segregation after heat treatment have resulted in single crystal alloys with significantly improved properties over conventionally cast blade materials.

Single crystal nickel-base superalloys are essentially two-phase composite materials (**2**) consisting of a large volume fraction (~60 to 65 per cent) of intermetallic γ' precipitates having the $L1_2$ crystal structure (**3**) interspersed in a coherent face-centred cubic γ solid solution nickel matrix. In the heat treated condition the γ' precipitates form periodic 3-dimensional arrays of cuboidal particles immersed in the γ matrix of face-centred nickel rich material, with the cuboid edges aligned along the (001) directions of the γ and γ' phases.

Recent evidence suggests that the deformation behaviour of the γ–γ' composite single crystal alloy is governed largely by the behaviour of the $L1_2$ ordered γ' phase. A summary of the constitutive behaviour of pure γ' Ni_3Al material which has the $L1_2$ crystal structure has been presented in the review paper by Pope and Ezz (**3**). They state that little is known regarding its creep behaviour, but a fairly complete consensus of opinion about its flow stress behaviour has been compiled. They also point out that Ni_3Al γ' material exhibits an anomalous increase of flow stress with increasing temperature up to about 760°C (1400°F) after which the flow stress rapidly decreases with further temperature increases. In two-phase γ–γ' alloys this behaviour is rationalized on the basis of cross-slip of screw dislocations from the octahedral crystallographic slip planes

to the cube slip planes when dislocation pairs enter and shear the γ' precipitates. Shearing the γ' precipitates, rather than dislocation bowing around the γ' precipitates, occurs due to the high volume fraction (65 per cent) of precipitate particles. Dislocations travel in pairs because single dislocations on the octahedral planes create an antiphase boundary (APB) trail where atoms of the structure are out-of-phase with each other. The energy associated with this APB is removed by the passage of another dislocation, which leaves a trail in which the atoms in the structure are in-phase with each other. Dislocations are therefore attracted to each other in pairs, in which there is an APB between each dislocation pair. The APB energy is anisotropic, being smaller on the cube planes than on the octahedral planes. Screw dislocations thus tend to cross-slip from the octahedral planes where the APB energy is high to the cube planes where it is low. As the octahedral dislocations enter the γ' particles they cross-slip onto the cube planes and are prevented from further motion by a pinning process (**3**). This pinning of the screw dislocations on the cube planes impedes the motion of the primary octahedral screw dislocations and raises the flow stress in the octahedral system. The octahedral flow stress thus increases with temperature since the rate at which the screw dislocations cross-slip and become pinned is governed by a diffusive process which increases with temperature.

Takeuchi and Kuramoto (**4**) proposed a theory for the anomalous increase of flow stress with temperature based on this diffusive cross-slip behaviour, and the theory was refined by Lall *et al.* (**5**). In the latter theory the octahedral $(a/2)[\bar{1}01]$ dislocation is an extended dislocation (**6**) consisting of two Shockley partial dislocation pairs $(a/6)[\bar{2}11] + (a/6)[\bar{1}\bar{1}2]$, separated by a stacking fault. In order to slip the pair must constrict into a single $(a/2)[\bar{1}01]$ dislocation. The constriction is aided by a shear stress on the (111) plane in the $[1\bar{2}1]$ direction, whereas a shear stress in the opposite direction extends the dislocation pair and tends to inhibit cross-slip. This 'core-width effect' gives rise to the tension–compression asymmetry observed in $L1_2$ crystal alloys. In recent work Paidar *et al.* (**7**)–(**8**) have noted that the tension–compression asymmetry disappears, according to the theory of Lall *et al.*, on the [012]–$[\bar{1}13]$ great circle in the standard [001]–[011]–$[\bar{1}11]$ stereographic triangle. However, experimental work shows that the tension–compression asymmetry disappears to the left of the [012]–$[\bar{1}13]$ great circle in the standard stereographic projection, and Paidar *et al.* (**7**) have modified the Lall *et al.* approach (**5**) to account for this effect by incorporating work originally due to Escaig (**9**) in their flow stress model. Below a temperature of 760°C (1400°F) the flow stress of pure Ni_3Al γ' material increases with increasing temperature due to the pinning of screw dislocations on the cube planes, but the overall macroscopic deformation is due to octahedral slip. No macroscopic cube slip is evident. However, above the peak temperature of 760°C (1400°F) the flow stress rapidly decreases with increasing temperature when large amounts of macroscopic cube slip occur in the γ' material. For [001] orientated specimens no cube slip can occur and it is

probable that the flow stress decreases with increasing temperature when the screw dislocations which have become pinned on the {100} cube planes by cross-slip from the {111} octahedral planes become unpinned (7)(10)–(12) as soon as they are formed and cross-slip back to the {111} octahedral planes.

Single crystal formulation

Constitutive modelling of nickel-base single crystal superalloys began with the work of Paslay *et al.* (12) in 1970. They proposed a theoretical formulation of steady state creep deformation based on crystallographic slip theory of face-centred cubic materials. In 1971 the theory was applied by Paslay *et al.* (13) to describe the creep behaviour of single crystal nickel-base superalloy tubes under biaxial tension. Steady state creep formulations suitable for the analysis of single crystals were used by Brown (14) in 1970 and by Hutchinson (15) in 1976 to predict the behaviour of polycrystalline materials whose aggregate consists of randomly orientated single crystal grains. Recently, Weng (16) has developed a single crystal creep formulation which accounts for transient (primary) as well as steady state (secondary) creep. However, in order to describe the combined plastic and creep behaviour of polycrystalline materials, Weng combines the rate-independent plastic and rate-dependent creep components in such a way that each component is governed by a separate constitutive relation; that is, plasticity and creep are assumed to be uncoupled phenomena.

In the decade of the seventies the creep and plastic responses of materials were combined into unified viscoplastic formulations (17)–(22). References (17)–(22) make extensive reference to the unified viscoplastic constitutive formulations of Bodner, Chaboche, Hart, Krempl, Cernocky, Krieg, Swearengen, Laflen, Lee, Zaverl, Stouffer, Miller, Robinson, Valanis and Walker. These formulations differ from steady state creep theories by introducing history dependent state variables to account for primary creep and plasticity. A single crystal formulation which accounts for the time-dependent viscoplastic behaviour of materials at elevated temperature can therefore be constructed by incorporating the steady state crystallographic creep model presented by Paslay *et al.* (12) into a unified viscoplastic formulation. The Takeuchi–Kuramoto cube cross-slip mechanism (4) and the Lall *et al.* (5)(7)(8)(10) Shockley partial tension–compression flow stress asymmetry mechanism may then be incorporated into the drag stress state variable of the unified viscoplastic constitutive formulation.

In order to model the constitutive behaviour of single crystal superalloys it is necessary to include both octahedral and cube crystallographic slip systems in the viscoplastic formulation. In the unit cell of a face-centred cubic crystal shown in Fig. 1, we denote by $\mathbf{m}_r^0$ a unit vector in the rth slip direction (of type ⟨110⟩), whilst $\mathbf{n}_r^0$ is a unit vector in the normal direction to the slip plane (of type {111}) of which $\mathbf{m}_r^0$ constitutes a slip direction. The four octahedral {111} planes and the twelve corresponding ⟨110⟩ slip directions (three on each plane)

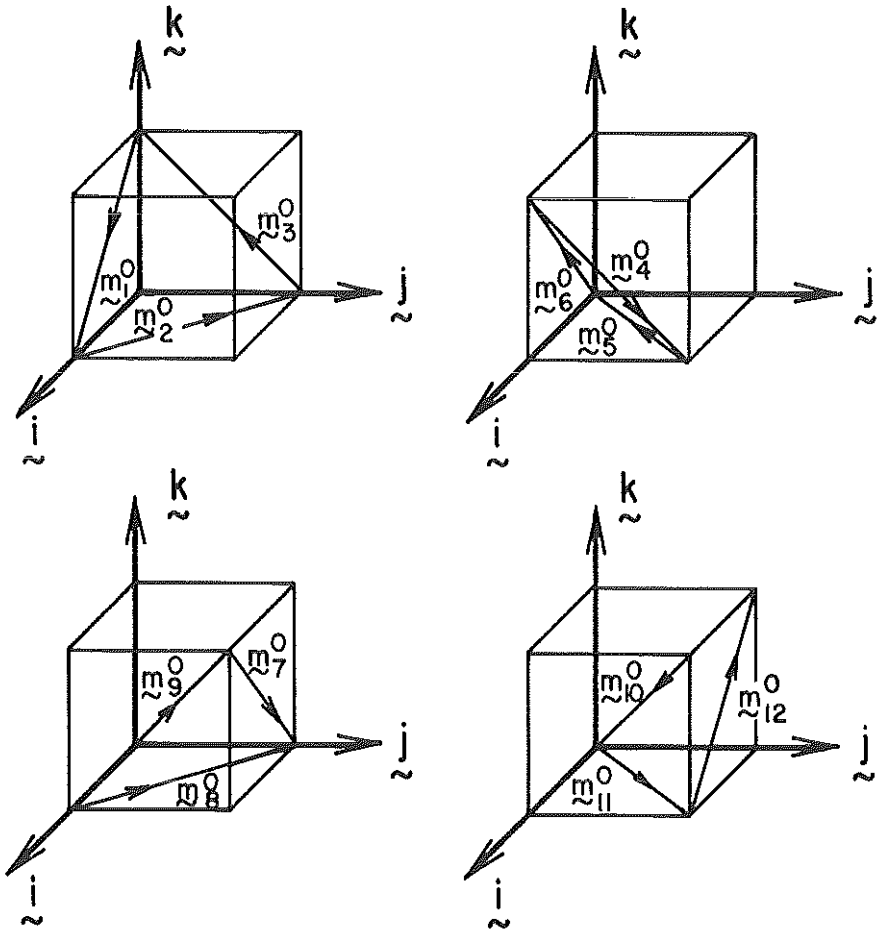

Fig 1 Octahedral planes and slip directions

are shown in Fig. 1. To each of the unit vectors $\mathbf{m}_r^0$ and $\mathbf{n}_r^0$ in the rth slip system there correspond perpendicular unit vectors, $\mathbf{z}_r^0$, given by $\mathbf{z}_r^0 = \mathbf{m}_r^0 \times \mathbf{n}_r^0$. The vector $\mathbf{z}_r^0$ corresponds to the octahedral $\langle 112 \rangle$ type slip directions and lies in the slip plane containing the vector $\mathbf{m}_r^0$, and the vectors, $\mathbf{m}_r^0$, $\mathbf{n}_r^0$, $\mathbf{z}_r^0$, form an orthogonal triad of unit vectors for the rth octahedral slip system. The corresponding unit vectors for the cube slip planes are denoted by $\mathbf{m}_r^c$ and $\mathbf{n}_r^c$, where the three cube $\{100\}$ planes and the six corresponding $\langle 110 \rangle$ slip directions (two on each plane) are shown in Fig. 2.

From the geometry of the unit cubic cell in Fig. 1 the twelve unit vectors for the octahedral slip system are given by

$$\mathbf{m}_1^0 = (\mathbf{i} - \mathbf{k})/\sqrt{2}, \quad \mathbf{m}_2^0 = (-\mathbf{i} + \mathbf{j})/\sqrt{2}, \quad \mathbf{m}_3^0 = (-\mathbf{j} + \mathbf{k})/\sqrt{2},$$
$$\mathbf{m}_4^0 = (\mathbf{j} - \mathbf{k})/\sqrt{2},$$
$$\mathbf{m}_5^0 = (-\mathbf{i} - \mathbf{j})/\sqrt{2}, \quad \mathbf{m}_6^0 = (\mathbf{i} + \mathbf{k})/\sqrt{2}, \quad \mathbf{m}_7^0 = (-\mathbf{i} - \mathbf{k})/\sqrt{2},$$
$$\mathbf{m}_8^0 = (\mathbf{i} - \mathbf{j})/\sqrt{2},$$
$$\mathbf{m}_9^0 = (\mathbf{j} + \mathbf{k})/\sqrt{2}, \quad \mathbf{m}_{10}^0 = (-\mathbf{j} - \mathbf{k})/\sqrt{2}, \quad \mathbf{m}_{11}^0 = (\mathbf{i} + \mathbf{j})/\sqrt{2},$$
$$\mathbf{m}_{12}^0 = (-\mathbf{i} + \mathbf{k})/\sqrt{2} \tag{1}$$

with unit normals

$$\mathbf{n}_1^0 = \mathbf{n}_2^0 = \mathbf{n}_3^0 = (\mathbf{i} + \mathbf{j} + \mathbf{k})/\sqrt{3}, \quad \mathbf{n}_4^0 = \mathbf{n}_5^0 = \mathbf{n}_6^0 = (-\mathbf{i} + \mathbf{j} + \mathbf{k})/\sqrt{3},$$
$$\mathbf{n}_7^0 = \mathbf{n}_8^0 = \mathbf{n}_9^0 = (-\mathbf{i} - \mathbf{j} + \mathbf{k})/\sqrt{3}, \quad \mathbf{n}_{10}^0 = \mathbf{n}_{11}^0 = \mathbf{n}_{12}^0 = (\mathbf{i} - \mathbf{j} + \mathbf{k})/\sqrt{3} \tag{2}$$

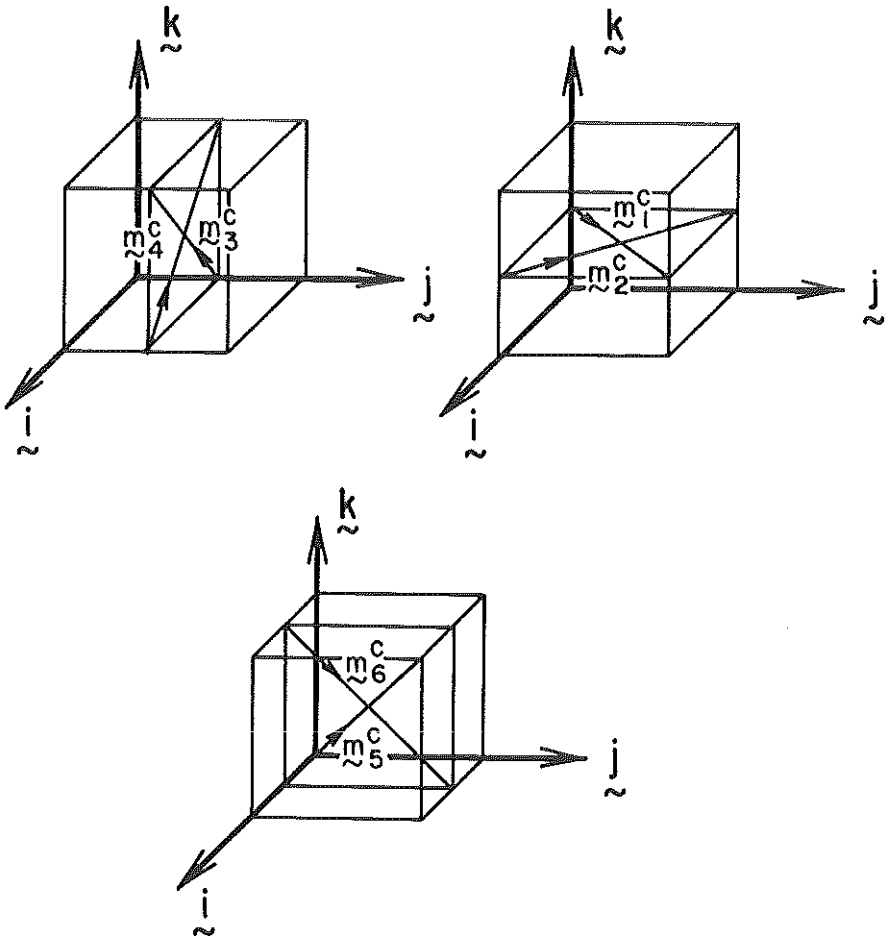

Fig 2 Cube planes and slip directions

and corresponding perpendicular vectors

$$\mathbf{z}_1^0 = (\mathbf{i} - 2\mathbf{j} + \mathbf{k})/\sqrt{6}, \quad \mathbf{z}_2^0 = (\mathbf{i} + \mathbf{j} - 2\mathbf{k})/\sqrt{6}, \quad \mathbf{z}_3^0 = (-2\mathbf{i} + \mathbf{j} + \mathbf{k})/\sqrt{6},$$
$$\mathbf{z}_4^0 = (2\mathbf{i} + \mathbf{j} + \mathbf{k})/\sqrt{6}, \quad \mathbf{z}_5^0 = (-\mathbf{i} + \mathbf{j} - 2\mathbf{k})/\sqrt{6}, \quad \mathbf{z}_6^0 = (-\mathbf{i} - 2\mathbf{j} + \mathbf{k})/\sqrt{6},$$
$$\mathbf{z}_7^0 = (-\mathbf{i} + 2\mathbf{j} + \mathbf{k})/\sqrt{6}, \quad \mathbf{z}_8^0 = (-\mathbf{i} - \mathbf{j} - 2\mathbf{k})/\sqrt{6},$$
$$\mathbf{z}_9^0 = (2\mathbf{i} - \mathbf{j} + \mathbf{k})/\sqrt{6},$$
$$\mathbf{z}_{10}^0 = (-2\mathbf{i} - \mathbf{j} + \mathbf{k})/\sqrt{6}, \quad \mathbf{z}_{11}^0 = (\mathbf{i} + \mathbf{j} - 2\mathbf{k})/\sqrt{6},$$
$$\mathbf{z}_{12}^0 = (\mathbf{i} + 2\mathbf{j} + \mathbf{k})/\sqrt{6} \tag{3}$$

where **i**, **j**, **k**, are unit vectors along the x, y, z, crystallographic axes. The six corresponding unit vectors for the cube slip system are given by

$$\mathbf{m}_1^c = (\mathbf{i} + \mathbf{j})/\sqrt{2}, \quad \mathbf{m}_2^c = (-\mathbf{i} + \mathbf{j})/\sqrt{2}, \quad \mathbf{m}_3^c = (\mathbf{i} + \mathbf{k})/\sqrt{2},$$
$$\mathbf{m}_4^c = (-\mathbf{i} + \mathbf{k})/\sqrt{2}, \quad \mathbf{m}_5^c = (\mathbf{j} + \mathbf{k})/\sqrt{2}, \quad \mathbf{m}_6^c = (-\mathbf{j} + \mathbf{k})/\sqrt{2} \tag{4}$$

with unit normals

$$\mathbf{n}_1^c = \mathbf{n}_2^c = \mathbf{k}, \quad \mathbf{n}_3^c = \mathbf{n}_4^c = \mathbf{j}, \quad \mathbf{n}_5^c = \mathbf{n}_6^c = \mathbf{i} \tag{5}$$

Figure 3 shows a single crystal bar specimen whose global axes are denoted

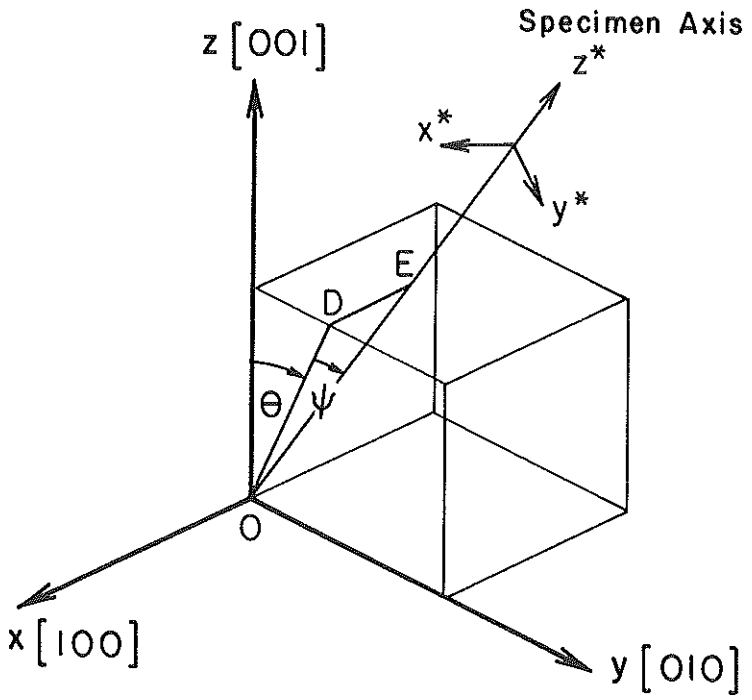

Fig 3 The position of the specimen axis within the standard stereographic triangle is defined by rotating Oz through an angle θ to OD and then by rotating OD through an angle ψ to OE

by x^*, y^*, z^*, and whose crystallographic axes are denoted by x, y, z. If Q_{ij} denotes the orthogonal tensor which rotates the crystallographic (unstarred) axes into the global (starred) axes, viz, $x_i^* = Q_{ij}x_j$, then the stress tensor σ_{ij} and the strain rate tensor $\dot{\varepsilon}_{ij}$ in the crystallographic axes may be obtained from the stress tensor σ_{ij}^* and the strain rate tensor $\dot{\varepsilon}_{ij}^*$ in the global system from the usual transformation relations

$$\sigma_{ij} = Q_{ik}\sigma_{kl}^* Q_{jl} \quad \text{and} \quad \dot{\varepsilon}_{ij} = Q_{ik}\dot{\varepsilon}_{kl}^* Q_{jl} \tag{6}$$

where, for the bar specimen shown in Fig. 3,

$$[\mathbf{Q}] = \begin{bmatrix} \cos\psi & 0 & -\sin\psi \\ \sin\theta\sin\psi & \cos\theta & \sin\theta\cos\psi \\ \cos\theta\sin\psi & -\sin\theta & \cos\theta\cos\psi \end{bmatrix} \tag{7}$$

The assumption is now made that any of the unified viscoplastic models discussed in references (**17**)–(**22**), when specialized to the case of shear deformation, is a valid constitutive relation in each of the twelve octahedral and six crystallographic slip directions. In the rth octahedral slip direction the Schmid resolved shear stress, π_{mn}^r, is obtained from the relation

$$\pi_{mn}^r = \mathbf{m}_r \cdot \boldsymbol{\sigma} \cdot \mathbf{n}_r \qquad (r = 1, 2, \ldots, 12) \tag{8}$$

where no sum over r is implied in equation (8) or in the equations which follow. When referred to the orthogonal system $\mathbf{m}_r^0$, $\mathbf{n}_r^0$, $\mathbf{z}_r^0$, the remaining components of the octahedral stress tensor can be written in the form

$$\begin{aligned} &\pi_{mm}^r = \mathbf{m}_r^0 \cdot \boldsymbol{\sigma} \cdot \mathbf{m}_r^0, \quad \pi_{nn}^r = \mathbf{n}_r^0 \cdot \boldsymbol{\sigma} \cdot \mathbf{n}_r^0, \quad \pi_{zz}^r = \mathbf{z}_r^0 \cdot \boldsymbol{\sigma} \cdot \mathbf{z}_r^0, \\ &\pi_{zm}^r = \pi_{mz}^r = \mathbf{m}_r^0 \cdot \boldsymbol{\sigma} \cdot \mathbf{z}_r^0, \quad \pi_{zn}^r = \pi_{nz}^r = \mathbf{n}_r^0 \cdot \boldsymbol{\sigma} \cdot \mathbf{z}_r^0 \qquad (r = 1, 2, \ldots, 12) \end{aligned} \tag{9}$$

The Schmid resolved shear stress in the rth cube slip direction, τ_r, is obtained from the corresponding relation

$$\tau_r = \tau_{mn}^r = \mathbf{m}_r^c \cdot \boldsymbol{\sigma} \cdot \mathbf{n}_r^c \qquad (r = 1, 2, \ldots, 6) \tag{10}$$

It is further assumed, in a manner analogous to the unified isotropic viscoplastic models, that the applicable relation governing the inelastic shear strain rate in the rth octahedral slip direction is

$$\dot{\gamma}_r = K_r^{-p}(\pi_r - \omega_r)|\pi_r - \omega_r|^{p-1} \qquad (r = 1, 2, \ldots, 12) \tag{11}$$

where K_r and ω_r denote the drag stress and the equilibrium (rest or back) stress in the rth octahedral slip direction. The stress component π_r is defined by the relation

$$\pi_r = \pi_{mn}^r + \alpha_{mm}\pi_{mm}^r + \alpha_{nn}\pi_{nn}^r + \alpha_{zz}\pi_{zz}^r + 2\alpha_{mz}\pi_{mz}^r + 2\alpha_{nz}\pi_{nz}^r \qquad (r = 1, 2, \ldots, 12) \tag{12}$$

in which the tensor whose components are α_{pq} represents the effect of the non-Schmid factors (**23**) upon the inelastic strain rate in the rth octahedral slip direction. For example, the term containing α_{nn} represents the effect of the

resolved stress, normal to the slip plane containing the rth octahedral slip direction, on the inelastic strain rate in the rth octahedral slip direction. Such terms can represent the effect of a pressure dependent inelastic strain rate. The dominant term in equation (12) is the Schmid type term containing the stress component π^r_{mn}; estimates of the magnitude of the non-Schmid type terms containing the tensor α_{pq} have been given by Asaro and Rice (**23**).

A power law expression is used in equation (11), but hyperbolic sine and exponential functional forms may also be used, as deemed appropriate for the material in question.

To complete the octahedral constitutive formulation it is necessary to specify the growth relations for the equilibrium and drag stress state variables. The equilibrium stress in the rth octahedral slip system may be assumed to evolve according to the evolution equation

$$\dot{\omega}_r = \varrho_1\dot{\gamma}_r - \varrho_2|\dot{\gamma}_r|\omega_r - \varrho_3|\omega_r|^{m-1}\omega_r \qquad (r = 1, 2, \ldots, 12) \tag{13}$$

The integral form of equation (13) is

$$\omega_r(t) = \varrho_1(t)\int_{\xi=0}^{t}(\partial\gamma_r/\partial\xi)\exp\left[-\int_{\zeta=\xi}^{t}\{\varrho_2(t)|\partial\gamma_r/\partial\zeta| + \varrho_3(t)|\omega_r(\zeta)|^{m(t)-1}\}\,d\zeta\right]d\xi \tag{14}$$

with $\varrho_1(t) = \varrho_1[\Theta(t)]$, etc., in contemplation of the fact that the material constants ϱ_1, ϱ_2, ϱ_3, and m may change with temperature Θ during a thermomechanical loading history. The integral of equation (13) should strictly be written in the form of equation (14) in which the material constant $\varrho_1(t)$ occurs inside the integral over ξ in the form $\varrho_1(\xi)$, and the material constants $\varrho_2(t)$, $\varrho_3(t)$, and $m(t)$ occur inside the integral over ζ in the forms $\varrho_2(\zeta)$, $\varrho_3(\zeta)$, and $m(\zeta)$. However, the integral form in equation (14) is preferred, since this form allows $\omega_r(t)$ to change instantaneously with temperature in the absence of inelastic deformation.

Upon differentiation with respect to time, equation (14) yields the relation

$$\dot{\omega}_r = \varrho_1\dot{\gamma}_r - \varrho_2|\dot{\gamma}_r|\omega_r - \varrho_3|\omega_r|^{m-1}\omega_r + X_r \qquad (r = 1, 2, \ldots, 12) \tag{15}$$

where

$$\begin{aligned} X_r(t) = {} & \{\dot{\varrho}_1(t)/\varrho_1(t)\}\omega_r(t) - \varrho_1(t)\int_{\xi=0}^{t}(\partial\gamma_r/\partial\xi) \\ & \times\left(\exp\left[-\int_{\zeta=\xi}^{t}\{\varrho_2(t)|\partial\gamma_r/\partial\zeta| + \varrho_3(t)|\omega_r(\zeta)^{m(t)-1}\}\,d\zeta\right]\right) \\ & \times\left(\int_{\chi=\xi}^{t}\{\dot{\varrho}_2(t)|\partial\gamma_r/\partial\chi| + \dot{\varrho}_3(t)|\omega_r(\chi)|^{m(t)-1} \right. \\ & \left. + \dot{m}(t)\varrho_3(t)|\omega_r(\chi)|^{m(t)-1}\log|\omega_r(\chi)|\}\,d\chi\right)d\xi \end{aligned} \tag{16}$$

Without the term X_r, the differential form of equation (13) shows that, in the absence of inelastic deformation (i.e., when $\dot{\gamma}_r$ is very small), the equilibrium stress, ω_r, changes only by thermal recovery. With X_r included in the differential equation the equilibrium stress, ω_r, can change with temperature in the absence of inelastic deformation.

The drag stress for the rth octahedral slip system may be assumed to grow according to the evolution equation

$$\dot{K}_r = \left(\sum_{k=1}^{12} [\beta_1\{q + (1 - q)\delta_{rk}\} - \eta_1(K_r - K_r^0)]|\dot{\gamma}_k| \right) - h_1(K_r - K_r^0)^s \qquad (r = 1, 2, \ldots, 12) \quad (17)$$

On each octahedral slip system the drag stress is assumed to harden according to the hardening modulus $h_{rk} = \beta_1\{q + (1 - q)\delta_{rk}\}$, which accounts for the latent hardening effects observed in single crystal materials. Numerous forms of the hardening moduli h_{rk} have been proposed in the literature, and a review of single crystal hardening moduli may be found in the article by Asaro (**24**). The particular form for h_{rk} adopted in equation (17) is due to Hutchinson (**25**); similar forms, which include the effects of finite deformation, were used by Asaro (**26**), and Peirce *et al.* (**27**), in finite element computations of finite deformation slip behaviour in single crystal materials. Further reviews concerning the hardening moduli can be found in the paper by Havner (**28**), which refers to previous work by Havner and his colleagues. Taylor hardening, in which each slip system hardens at equal rates, can be simulated with the Hutchinson modulus, h_{rk}, by setting $q = 1$.

The initial value of the drag stress in the rth octahedral slip system, K_r^0, defined by the relation

$$K_r^0 = K_1 + K_2 \exp\,[\varrho_4 \pi_{nz}^r + \varrho_5|\Psi_r|] \qquad (r = 1, 2, \ldots, 12) \quad (18)$$

accounts for the tension–compression asymmetry of the flow stress observed in single crystal nickel-base superalloys. The shear stress component Ψ_r is the resolved shear stress on the cube crystallographic slip planes in the direction of the octahedral slip vector $\mathbf{m}_r^0$. According to the Takeuchi–Kuramoto cross-slip model this stress component is the driving force which causes the primary dislocations on the {111} octahedral planes to cross-slip onto the {100} cube planes where they form sessile segments. The interaction between the primary octahedral dislocations and the pinned sessile segments increases the flow stress in the octahedral system. An increase in temperature enhances the cross-slip process and is, therefore, responsible for the increase in flow or yield stress with temperature in the octahedral slip system. In a unified viscoplastic formulation the yield or flow stress is analogous to the drag stress state variable and the constants ϱ_4, ϱ_5, and K_2 therefore increase with temperature, Θ (in Takeuchi and Kuramoto's model K_2 increases according to the relation $\exp\,[-H/k\Theta]$). This provides the anomalous increase of flow stress with increasing temperature found in superalloy crystals which have γ' precipitate

particles possessing the $L1_2$ superlattice crystal structure. Since the magnitude of the stress component Ψ_r occurs in equation (18), the increase in yield (flow) stress due to the cube cross-slip process is the same for both tension and compression testing of a single crystal bar specimen.

The effect of the Shockley partial dislocations on yield stress asymmetry is recognized explicitly in the 'core-width' term containing the stress component π^r_{nz} in the initial drag stress term in equation (18). This shear stress component in the octahedral ⟨112⟩ type directions can extend or constrict the Shockley partial dislocations and changes sign when the applied stress state changes from tension to compression in a single crystal bar specimen, as proposed by Lall *et al.* (3)(5). The expression for π^r_{nz} is given in equation (9), whilst the cube cross-slip component, Ψ_r, is obtained from the following relations

$$\begin{aligned}
&\Psi_1 = \mathbf{m}^0_1\cdot\boldsymbol{\sigma}\cdot\mathbf{j}, \quad \Psi_2 = \mathbf{m}^0_2\cdot\boldsymbol{\sigma}\cdot\mathbf{k}, \quad \Psi_3 = \mathbf{m}^0_3\cdot\boldsymbol{\sigma}\cdot\mathbf{i}, \quad \Psi_4 = \mathbf{m}^0_4\cdot\boldsymbol{\sigma}\cdot\mathbf{i}\\
&\Psi_5 = \mathbf{m}^0_5\cdot\boldsymbol{\sigma}\cdot\mathbf{k}, \quad \Psi_6 = \mathbf{m}^0_6\cdot\boldsymbol{\sigma}\cdot\mathbf{j}, \quad \Psi_7 = \mathbf{m}^0_7\cdot\boldsymbol{\sigma}\cdot\mathbf{j}, \quad \Psi_8 = \mathbf{m}^0_8\cdot\boldsymbol{\sigma}\cdot\mathbf{k}\\
&\Psi_9 = \mathbf{m}^0_9\cdot\boldsymbol{\sigma}\cdot\mathbf{i}, \quad \Psi_{10} = \mathbf{m}^0_{10}\cdot\boldsymbol{\sigma}\cdot\mathbf{i}, \quad \Psi_{11} = \mathbf{m}^0_{11}\cdot\boldsymbol{\sigma}\cdot\mathbf{k}, \quad \Psi_{12} = \mathbf{m}^0_{12}\cdot\boldsymbol{\sigma}\cdot\mathbf{j}
\end{aligned} \tag{19}$$

The expressions containing the material constants η_1 and h_1 in equation (17) represent the dynamic and thermal recovery terms of the drag stress evolution equations in which the recovery is assumed to take place towards the initial value of the drag stress, K^0_r. In integral form, the drag stress may be written as

$$\begin{aligned}
K_r(t) = K^0_r(t) + \sum_{k=1}^{12} \beta_1(t)[q(t) + (1 - q(t))\delta_{rk}] \int_{\xi=0}^{t} |\partial\gamma_k/\partial\xi| \\
\times \exp\left[-\int_{\zeta=\xi}^{t} \{\eta_1(t) \sum_{i=1}^{12} |\partial\gamma_i/\partial\zeta| \right. \\
\left. + h_1(t)[K_r(\zeta) - K^0_r(\zeta)]^{s(t)-1}\} \, d\zeta \right] d\xi
\end{aligned} \tag{20}$$

where the material constants β_1, q, η_1, h_1, and s depend on time through their dependence on temperature according to the relations $\beta_1(t) = \beta_1[\Theta(t)]$, etc. The function $K^0_r(t)$ also depends on time through the dependence of the material constants K_1 and K_2 on temperature. Strictly speaking, the terms containing β_1 and q should occur inside the integral sign, with t replaced by ξ, and the terms containing η_1, h_1, and s should occur with t replaced by ζ, but, as in the case of the equilibrium stress, the form of equation (20) is preferred, since this form allows $K_r(t)$ to change instantaneously with temperature in the absence of inelastic deformation.

The integral forms of the equilibrium stress and drag stress components listed in equations (14) and (20) change instantaneously with temperature, since the material constants which occur in the integral forms are evaluated at the current temperature. The differential forms of the integrals in (14) and (20) will involve terms such as X_r, containing the derivatives of the material constants with temperature, in addition to the terms already present in equations (13) and (17). These extra terms allow the state variables to change with temperature in

the absence of inelastic deformation. In a yield surface plasticity theory a change in the equilibrium (rest or back) stress corresponds to a kinematic shift of the centre of the yield surface, while a change in the drag stress corresponds to an isotropic change in the radius of the yield surface. In the absence of inelastic deformation both the yield surface centre and its radius can change instantaneously with temperature, and the integral forms of the state variables in equations (14) and (20) are the corresponding analogues in the unified constitutive formulation.

A similar set of constitutive equations is assumed to hold for the case of crystallographic cube slip. The inelastic shear strain rate in the rth cube slip direction is assumed to have the form

$$\dot{\alpha}_r = L_r^{-t}(\tau_r - \Omega_r)|\tau_r - \Omega_r|^{t-1} \qquad (r = 1, 2, \ldots, 6) \tag{21}$$

where L_r and Ω_r denote the drag stress and the equilibrium (rest or back) stress in the rth cube slip direction. These state variables are assumed to evolve according to the evolution equations

$$\dot{\Omega}_r = \varrho_6\dot{\alpha}_r - \varrho_7|\dot{\alpha}_r|\Omega_r - \varrho_8|\Omega_r|^{n-1}\Omega_r \qquad (r = 1, 2, \ldots, 6) \tag{22}$$

and

$$\dot{L}_r = \left\{\sum_{k=1}^{6}[\beta_2 - \eta_2(L_r - L_r^0)]|\dot{\alpha}_k|\right\} - h_2(L_r - L_r^0)^u \qquad (r = 1, 2, \ldots, 6) \tag{23}$$

where $L_r^0 = L_1$ is the initial constant value of the drag stress component on the rth cube slip system. No latent hardening or asymmetry terms are included in the cube slip formulation since cube slip operates only at elevated temperatures where latent hardening and yield stress asymmetry are absent.

The integral forms of the equilibrium and drag stress state variables for the cube slip systems may be written as

$$\Omega_r(t) = \varrho_6(t)\int_{\xi=0}^{t}(\partial\alpha_r/\partial\xi) \times \exp\left[-\int_{\zeta=\xi}^{t}\{\varrho_7(t)|\partial\alpha_r/\partial\zeta| + \varrho_8(t)|\Omega_r(\zeta)|^{n(t)-1}\}\,d\zeta\right]d\xi \tag{24}$$

and

$$L_r(t) = L_r^0(t) + \sum_{k=1}^{6}\beta_2(t)\int_{\xi=0}^{t}|\partial\alpha_k/\partial\xi| \times \exp\left[-\int_{\zeta=\xi}^{t}\left\{\eta_2(t)\sum_{i=1}^{6}|\partial\alpha_i/\partial\zeta| + h_2(t)[L_r(\zeta) - L_r^0(\zeta)]^{u(t)-1}\right\}d\zeta\right]d\xi \tag{25}$$

and the differential forms of these integral equations are to be used in thermomechanical calculations where both strain and temperature vary with time.

The shear slip strain rates may now be resolved into the crystallographic system and summed for each slip system to obtain the inelastic strain rate tensor, $\dot{c}_{ij}$, with respect to the crystal axes in the form

$$\dot{c}_{ij} = \sum_{r=1}^{12} a_{ij}^{r}\dot{\gamma}_r + \sum_{r=1}^{6} b_{ij}^{r}\dot{\alpha}_r \tag{26}$$

where

$$a_{ij}^{r} = \tfrac{1}{2}[(\mathbf{i}\cdot\mathbf{n}_r^0)(\mathbf{m}_r^0\cdot\mathbf{j}) + (\mathbf{i}\cdot\mathbf{m}_r^0)(\mathbf{n}_r^0\cdot\mathbf{j})]$$

and

$$b_{ij}^{r} = \tfrac{1}{2}[(\mathbf{i}\cdot\mathbf{n}_r^c)(\mathbf{m}_r^c\cdot\mathbf{j}) + (\mathbf{i}\cdot\mathbf{m}_r^c)(\mathbf{n}_r^c\cdot\mathbf{j})] \tag{27}$$

Finally, the stress rate tensor with respect to the crystallographic axes is determined from the relation

$$\dot{\sigma}_{ij} = D_{ijkl}^{c}(\dot{\varepsilon}_{kl} - \dot{c}_{kl}) + \dot{D}_{ijkl}^{c}(\varepsilon_{kl} - c_{kl}) \tag{28}$$

where D_{ijkl}^{c} is the anisotropic elasticity tensor for the face-centred cubic crystal referred to the crystallographic axes. The variables can now be updated in the Euler forward difference form

$$\begin{aligned}
&\sigma_{ij}(t+\Delta t) = \sigma_{ij}(t) + \dot{\sigma}_{ij}(t)\Delta t, \quad \varepsilon_{ij}(t+\Delta t) = \varepsilon_{ij}(t) + \dot{\varepsilon}_{ij}(t)\Delta t\\
&c_{ij}(t+\Delta t) = c_{ij}(t) + \dot{c}_{ij}(t)\Delta t,\\
&\omega_r(t+\Delta t) = \omega_r(t) + \dot{\omega}_r(t)\Delta t, \quad \Omega_r(t+\Delta t) = \Omega_r(t) + \dot{\Omega}_r(t)\Delta t,\\
&K_r(t+\Delta t) = K_r(t) + \dot{K}_r(t)\Delta t,\\
&L_r(t+\Delta t) = L_r(t) + \dot{L}_r(t)\Delta t, \quad \gamma_r(t+\Delta t) = \gamma_r(t) + \dot{\gamma}_r(t)\Delta t,\\
&\alpha_r(t+\Delta t) = \alpha_r(t) + \dot{\alpha}_r(t)\Delta t,\\
&\sigma_{ij}^{*}(t+\Delta t) = Q_{ki}\sigma_{kl}(t+\Delta t)Q_{lj}, \quad \varepsilon_{ij}^{*}(t+\Delta t) = Q_{ki}\varepsilon_{kl}(t+\Delta t)Q_{lj}
\end{aligned} \tag{29}$$

The preceding discussion has focused on slip which occurs on the {100} cube planes in the ⟨110⟩ type directions and on the {111} octahedral planes in the ⟨110⟩ type directions of face-centred cubic nickel-base superalloys. Leverant *et al.* **(29)**–**(30)** found that slip occurs under primary creep conditions at low stress levels on the {111} planes in the ⟨112⟩ type directions of the single crystal alloy Mar–M200. We have not yet determined if this is the case for PWA 1480, but attempts at fitting creep data at low stress levels with material constants obtained from high strain rate tests (10^{-3}–10^{-5} per second) have not proved successful. These results suggest that either: (a) the creep slip mode mechanism differs from the high strain rate slip mode mechanism and additional terms reflecting creep in the ⟨112⟩ type directions are needed in the inelastic strain rate relation in equation (26); or (b) the power law expressions for the inelastic shear strain rates in equations (11) and (21) are inadequate over the range of strain rates extending from creep conditions (10^{-7} per second) to high strain rates experienced in typical thermomechanical loading conditions for turbine blades (10^{-3} per second).

For each different slip system the foregoing theory is altered only by virtue of having different slip and normal vectors defining the triad $\mathbf{m}_r$, $\mathbf{n}_r$, and $\mathbf{z}_r$. The total inelastic strain rate may then be written as the sum of the inelastic strain rates due to each slip system.

Initial experiments and simulations

The determination of model constants and model verification is being carried out using an elevated temperature 871°C (1600°F) tension–torsion servohydraulic test set-up developed as part of a fatigue research program (NASA NAG3-160). This system comprises a 2500 Nm, 250 kN servohydraulic tension–torsion machine differing from commercial machines only by virtue of a University of Connecticut-developed load frame made from a large die set. Force and torque are measured with a conventional strain gauge load–torque cell, whilst strain is measured by a University of Connecticut-designed extensometer that utilizes high temperature noncontacting displacement probes. This extensometer, shown in Fig. 4, allows testing in excess of 871°C (1600°F) without any need to cool the extensometer. The machine is controlled with a DEC LSI-1123 microcomputer using software developed under the current research program. This software allows a wide variety of tests to be run, including tests involving a sudden change in strain rate (**31**), known to be useful

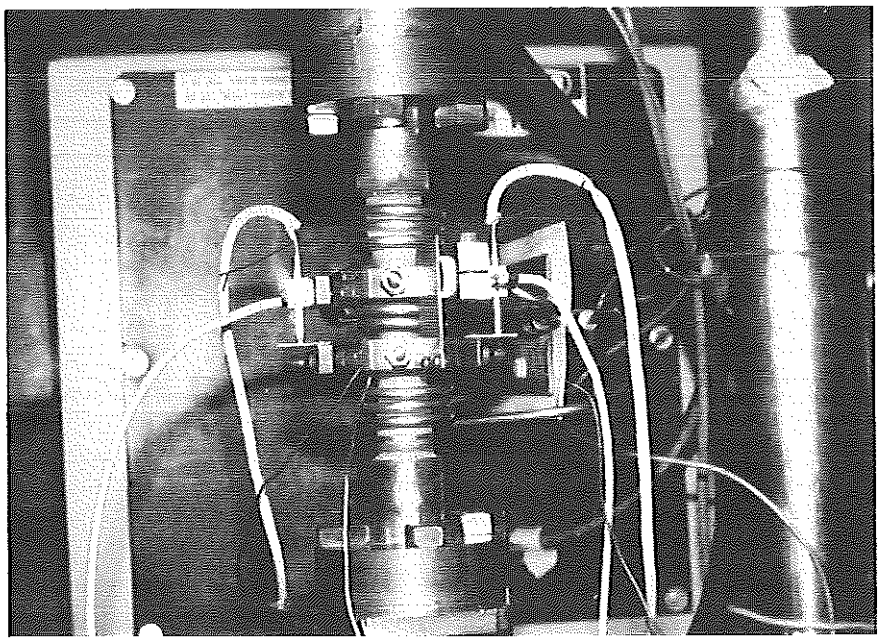

Fig 4 Single crystal tubular specimen with extensometer and induction heater during a biaxial test at 871°C (1600°F)

in assessing the magnitude of the drag stress state variable used in the anisotropic constitutive model. Strain holds can also be inserted into a strain history and this is particularly useful in assessing the magnitude of the equilibrium (back or rest) stress state variable (**32**). The material being tested is a high volume fraction (65 per cent) γ' single crystal material, PWA 1480, supplied by Pratt & Whitney.

The preliminary tests reported here represent the first biaxial tension–torsion tests run on this type of single crystal alloy. Biaxial testing has the special advantage that orientation effects may be studied by varying the stress state as opposed to growing specimens in a wide variety of configurations as is usually done for uniaxial testing. Preliminary experiments with this material have shown that at 871°C (1600°F) it is possible to return the material to the same deformation state by applying a few repeated cycles of almost any strain history. As a result a large number of different types of tests can be run on a single specimen. Tension tests, when combined with torsion results, provide a powerful and easy way to determine the relative proportions of octahedral slip and cube slip, which is vital to the success of the proposed model. For example, in tension–compression testing of the [001] orientated tubular specimen, the resolved shear stresses on the cube slip planes are zero, and only octahedral slip is activated. However, during torsional deformation, both the octahedral and cube slip systems are activated.

Many materials are known to cyclically harden (**33**)–(**34**) to a much greater degree in non-proportional loading, and it is important to determine if PWA 1480 exhibits this common behaviour. A test series was run in which a torsional loop was taken followed by cycling with a torsion to tension strain ratio of 1.5 and with tension and torsion 90 degrees out-of-phase. This type of non-proportional cycling is known to be especially effective (**33**)–(**34**) in producing extra hardening. For PWA 1480 at 871°C (1600°F) the torsional loops before and after this cycling are so similar as to be nearly indistinguishable, demonstrating that there is no extra hardening in this alloy for non-proportional loading. We take this as an indication that latent hardening effects are absent at elevated temperature in this single crystal alloy. Similar results for the superalloys B1900 + Hf and Mar–M247 have been reported by Lindholm *et al.* (**19**) and for René 80 by Ramaswamy *et al.* (**22**) at both elevated temperature and room temperature.

It may also be possible that latent hardening effects are present in superalloys with the γ–γ' structure, and that the motion of dislocations in and around the γ–γ' interfaces is such that many or all of the latently hardened octahedral and cube slip systems are activated and sampled locally by the interface dislocations. This sampling of the latently hardened slip systems by the dislocations normally occurs in single phase alloys only when the material is subjected to non-proportional straining conditions. Thus, for superalloys with the two phase γ–γ' structure, all the extra latent hardening may take place locally under macroscopic uniaxial straining conditions. No extra hardening under non-

proportional strain histories would then be observed since the material would reach the fully hardened condition under proportional uniaxial straining due to the heterogeneity of the material. It is supposed, in this explanation, that the extra hardening normally found in copper, aluminium, steel, Hastelloy-X, etc., when cycled under out-of-phase non-proportional cyclic loading conditions, is due to the fact that the rotating principal stress state samples all of the slip systems, including those that have experienced latent hardening. Under uniaxial conditions in such materials, the latently hardened systems are not sampled since the principal stress state does not rotate during straining, and the extra hardening is not observed.

The constitutive model contains material constants which vary with temperature. These constants must be determined for both the octahedral and cube slip systems. When a cylindrical tubular specimen, which has its cylindrical axis orientated within the standard [001]–[011]–[$\bar{1}$11] stereographic triangle, is loaded in tension and compression the resolved shear stresses on the octahedral and cube crystallographic planes are generally different. This makes the determination of the material constants a very difficult task. However, when the cylindrical specimen is orientated with its axis aligned along either the [001], [011] or [$\bar{1}$11] crystallographic directions the inelastic strain rates in each of the operative octahedral slip systems are equal, and the corresponding inelastic strain rates in each of the operative cube slip systems are also equal, though they differ from the octahedral values. This simplifies the form of the uniaxial constitutive relations dramatically, and the uniaxial constitutive relations

Table 1 Uniaxial constitutive relation for bar specimens orientated in the [001], [011], and [$\bar{1}$11] directions

$$\dot{\sigma} = \mathfrak{B}(\dot{\varepsilon} - \dot{c})$$

$$\mathfrak{C} = \{(D^c_{1111} + D^c_{1122})/[(D^c_{1111} + 2D^c_{1122})(D^c_{1111} - D^c_{1122})] + [(1/D^c_{1212}) - 2/(D^c_{1111} - D^c_{1122})]\mathfrak{S}\}^{-1}$$

$$\dot{c} = \mathfrak{B}K^{-p}(\mathfrak{D}\sigma - \omega)|\mathfrak{D}\sigma - \omega|^{p-1} + \mathfrak{C}L^{-t}(\mathfrak{F}\sigma - \Omega)|\mathfrak{F}\sigma - \Omega|^{t-1}$$

$$\dot{\gamma} = K^{-p}(\mathfrak{D}\sigma - \omega)|\mathfrak{D}\sigma - \omega|^{p-1}, \quad \dot{\alpha} = L^{-t}(\mathfrak{F}\sigma - \Omega)|\mathfrak{F}\sigma - \Omega|^{t-1}$$

$$\dot{\omega} = \varrho_1\dot{\gamma} - \varrho_2|\dot{\gamma}|\omega - \varrho_3|\omega|^{m-1}\omega, \quad \dot{\Omega} = \varrho_6\dot{\alpha} - \varrho_7|\dot{\alpha}|\Omega - \varrho_8|\Omega|^{n-1}\Omega$$

$$\dot{K} = [\beta_1\{1 + (\mathfrak{G} - 1)q\}/\mathfrak{G} - \eta_1(K - K^0)]\mathfrak{G}|\dot{\gamma}| - h_1(K - K^0)^s$$

$$\dot{L} = [\beta_2 - \eta_2(L - L^0)]\mathfrak{R}|\dot{\alpha}| - h_2(L - L^0)^u$$

$$L^0 = L_1 \quad \text{and} \quad K^0 = K_1 + K_2 \exp[\varrho_4\mathfrak{P}\sigma + \varrho_5\mathfrak{Q}|\sigma|]$$

[001] constants	[011] constants	[$\bar{1}$11] constants
$\mathfrak{S} = 0$	$\mathfrak{S} = 1/4$	$\mathfrak{S} = 1/3$
$\mathfrak{B} = 8/\sqrt{6}$	$\mathfrak{B} = 4/\sqrt{6}$	$\mathfrak{B} = 4/\sqrt{6}$
$\mathfrak{C} = 0$	$\mathfrak{C} = \sqrt{2}$	$\mathfrak{C} = \sqrt{2}$
$\mathfrak{D} = 1/\sqrt{6}$	$\mathfrak{D} = 1/\sqrt{6}$	$\mathfrak{D} = \sqrt{6}/9$
$\mathfrak{F} = 0$	$\mathfrak{F} = 1/(2\sqrt{2})$	$\mathfrak{F} = 2/\sqrt{18}$
$\mathfrak{G} = 8$	$\mathfrak{G} = 4$	$\mathfrak{G} = 6$
$\mathfrak{R} = 0$	$\mathfrak{R} = 4$	$\mathfrak{R} = 3$
$\mathfrak{P} = 1/\sqrt{18}$	$\mathfrak{P} = -1/\sqrt{18}$	$\mathfrak{P} = -2/(3\sqrt{18})$
$\mathfrak{Q} = 0$	$\mathfrak{Q} = 1/(2\sqrt{2})$	$\mathfrak{Q} = \sqrt{2/3}$

corresponding to the three corners of the stereographic triangle, viz. [001], [011] and [$\bar{1}$11], are given in Table 1. The factors in the uniaxial form of the constitutive relation which vary with orientation are written as German capitals. A similar simplification takes place for the shearing of a cube of material with its cube axes orientated along the crystallographic axes, and this constitutive relation for shear is given in Table 2. This relation can be used to simulate the behaviour of a tubular specimen, with its axis orientated along the [001] direction, when subjected to a twist about this axis.

Most of the tubular specimens are orientated with their cylindrical axes along the [001] crystallographic direction. When pulled in the axial direction the resolved shear stresses on the crystallographic cube planes are zero and only octahedral slip occurs. Material constants for the octahedral slip component of the constitutive model are most conveniently derived from the data obtained by loading these specimens in uniaxial tension and compression at a constant strain amplitude and at different strain rates. Figure 5(a) shows the experimental steady state uniaxial hysteresis data for PWA 1480 at 871°C (1600°F) at strain rates of 10^{-3}, 10^{-4}, and 10^{-5} per second in the [001] orientation, and Fig. 5(b) shows the corresponding loops predicted with the constitutive model which agree well with the data. Since the octahedral material constants are obtained from the experimental [001] data in Fig. 5(a) the agreement between theory and test merely shows how well the theoretical formulation can correlate the experimental data in this crystallographic orientation.

Predictions of steady state uniaxial hysteresis loops at strain rates of 5×10^{-3}, 10^{-3}, 10^{-4}, and 10^{-5} per second for PWA 1480 specimens orientated in the [$\bar{1}$11] crystallographic direction are also shown in Fig. 5(b) and exhibit good agreement with the experimental results in Fig. 5(a). Again, good agreement is to be expected, since the material constants for the cube slip systems were obtained by matching the theoretical predictions of the [$\bar{1}$11] hysteresis loops with the experimental results. The procedure for obtaining the material constants first

Table 2 Constitutive relation for shear of a [001] orientated specimen

$$\sigma = \sigma_{12}, \quad \varepsilon = \varepsilon_{12}, \quad c = c_{12}$$
$$\dot{\sigma} = 2D^{s}_{1212}(\dot{\varepsilon} - \dot{c})$$
$$\dot{c} = 2(\dot{\gamma}_1 + \dot{\gamma}_2)/\sqrt{6} + \sqrt{2}\dot{\alpha}$$
$$\dot{\gamma}_1 = K_1^{-p}(\sigma/\sqrt{6} - \omega_1)|\sigma/\sqrt{6} - \omega_1|^{p-1}, \quad \dot{\gamma}_2 = K_2^{-p}(\sigma/\sqrt{6} - \omega_2)|\sigma/\sqrt{6} - \omega_2|^{p-1}$$
$$\dot{\omega}_1 = \varrho_1\dot{\gamma}_1 - \varrho_2|\dot{\gamma}_1|\omega_1 - \varrho_3|\omega_1|^{m-1}\omega_1, \quad \dot{\omega}_2 = \varrho_1\dot{\gamma}_2 - \varrho_2|\dot{\gamma}_2|\omega_2 - \varrho_3|\omega_2|^{m-1}\omega_2$$
$$\dot{\alpha} = L^{-t}(\sigma/\sqrt{2} - \Omega)|\sigma/\sqrt{2} - \Omega|^{t-1}, \quad \dot{\Omega} = \varrho_6\dot{\alpha} - \varrho_7|\dot{\alpha}|\Omega - \varrho_8|\Omega|^{n-1}\Omega$$
$$\dot{K}_1 = 4[\beta_1(1 + 3q)/4 - \eta_1(K_1 - K_1^0)]|\dot{\gamma}_1| - h_1(K_1 - K_1^0)^s$$
$$\dot{K}_2 = 4[\beta_1(1 + 3q)/4 - \eta_1(K_2 - K_2^0)]|\dot{\gamma}_2| - h_1(K_2 - K_2^0)^s$$
$$\dot{L} = 4[\beta_2 - \eta_2(L - L^0)]|\dot{\alpha}| - h_2(L - L^0)^u$$
$$L^0 = L_1$$
$$K_1^0 = K_1 + K_2 \exp[\varrho_4\sigma/(3\sqrt{2}) + \varrho_5|\sigma/\sqrt{2}|]$$
$$K_2^0 = K_1 + K_2 \exp[-\varrho_4\sigma/(3\sqrt{2}) + \varrho_5|\sigma/\sqrt{2}|]$$

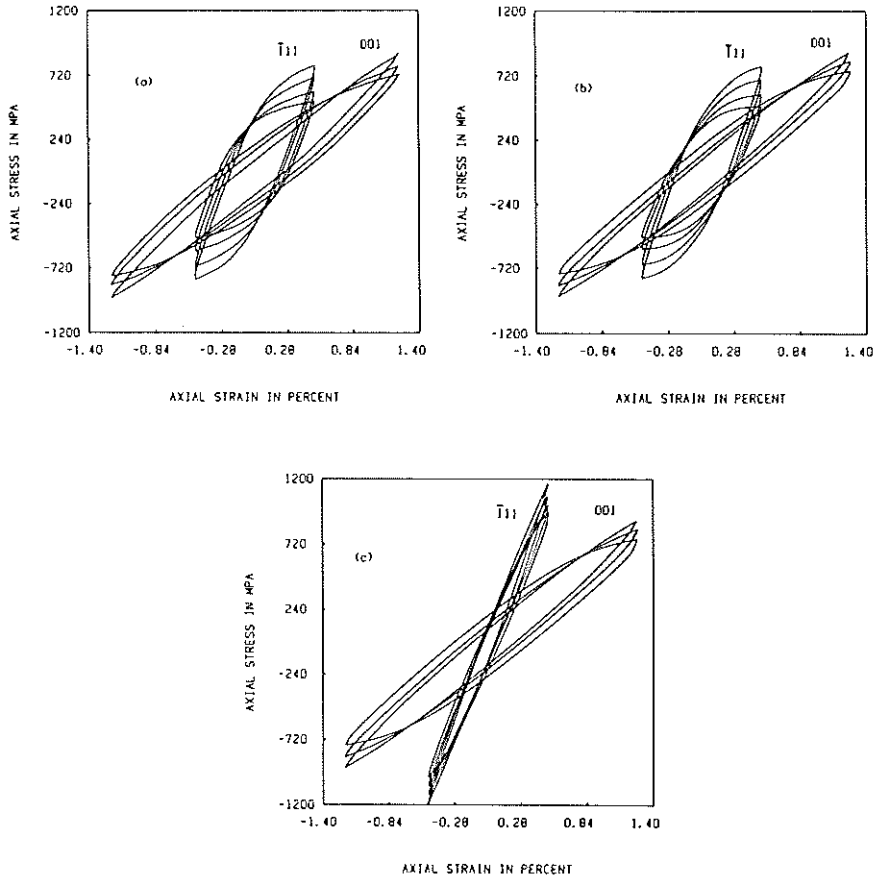

Fig 5 Steady state hysteresis loops at various strain rates in the [001] and [$\bar{1}$11] directions at 871°C (1600°F): (a) experimental; (b) theoretical correlations using octahedral and cube slip with the material constants in Table 3; (c) theoretical correlations using only octahedral slip. Strain rates are 10^{-3}, 10^{-4}, and 10^{-5} per second in the [001] direction and 5×10^{-3}, 10^{-3}, 10^{-4}, and 10^{-5} per second in the [$\bar{1}$11] direction

matches the theoretical and experimental results for the [001] orientation, where cube slip is inoperative and the values of the cube material constants are not required. Then, knowing the octahedral material constants, the values of the cube material constants are found by matching the theoretical and experimental results for the [$\bar{1}$11] orientation, where both slip systems are operative. The resulting predictions in Figs 5(a) and 5(b) are, therefore, a reflection of the correlative capability of the theory at these two crystallographic orientations. The correlative capability of the theoretical formulation is found to be adequate for the [001] and [$\bar{1}$11] orientations when both octahedral and cube slip are incorporated into the crystallographic slip model.

Such is not the case if only octahedral slip is used in the theoretical formulation. In Fig. 5(c), cube slip has been omitted from the theoretical formulation. As may be expected, the results for the [001] orientation are not affected since cube slip is inoperative for this orientation (the resolved shear stresses on all six cube slip systems are zero in the [001] orientation). However, when the theoretical formulation with only octahedral slip is used in an attempt to correlate the $[\bar{1}11]$ hysteresis data, the result is a failure. The predicted $[\bar{1}11]$ hysteresis loops are observed to be much too narrow in Fig. 5(c). This failure to correlate the $[\bar{1}11]$ data arises from the fact that cube slip is the dominant slip mode in the $[\bar{1}11]$ orientation under uniaxial loading conditions, and the suppression of inelasticity due to cube slip leaves only the weakly active octahedral systems. The octahedral systems cannot supply enough inelastic behaviour to correlate the $[\bar{1}11]$ data without the additional inelastic behaviour of the cube slip systems.

With the material constants now fixed from the preceding theoretical correlations with the [001] and $[\bar{1}11]$ experimental data, the constitutive model can then be used to see how well it can predict experimental results which were *not used* in determining the material constants. This allows the predictive capability of the constitutive formulation to be assessed. In Figs 6(a) and 6(b) the steady state uniaxial hysteresis loops for strain rates of 10^{-2}, 10^{-3}, and 10^{-5} per second in the [011] crystallographic orientation at 871°C (1600°F) are compared. The calculated loops agree favourably with the experimental loops, indicating that the predictive capability of the slip theory formulation containing both octahedral and cube slip systems is good. Again, if only octahedral slip is used in the constitutive formulation, the predicted loops in Fig. 6c appear much too narrow due to the lack of cube slip inelasticity.

Figure 7(a) shows steady state torsional hysteresis loops carried out at strain rates of 10^{-3}, 10^{-4}, and 5×10^{-5} per second at a strain range of 0.6 per cent at 871°C (1600°F). Predictions with the combined octahedral and cube slip model, using the material constants derived from the [001] and $[\bar{1}11]$ correlations, are shown in Fig. 7(b). If only octahedral slip is included in the constitutive model the predicted loops, shown in Fig. 6(b), are again much too narrow due to the suppression of cube slip inelasticity.

From these correlations and predictions it is clear that uniaxial specimens in several orientations are needed to obtain both the octahedral and cube material constants in the constitutive formulation. However, if torsional tube specimens are available, the octahedral material constants can be obtained from uniaxial straining of a tube orientated with its cylindrical axis along the [001] orientation, since cube slip is absent in this condition. Torsion tests on such tubular specimens will involve both octahedral and cube slip, and can be used to determine the cube slip constants once the octahedral constants have been determined from the [001] uniaxial deformation of the specimen. Comparison of the predicted torsional loops (using octahedral slip only) with the experimental loops can be used to detect the occurrence of cube slip which is usually found

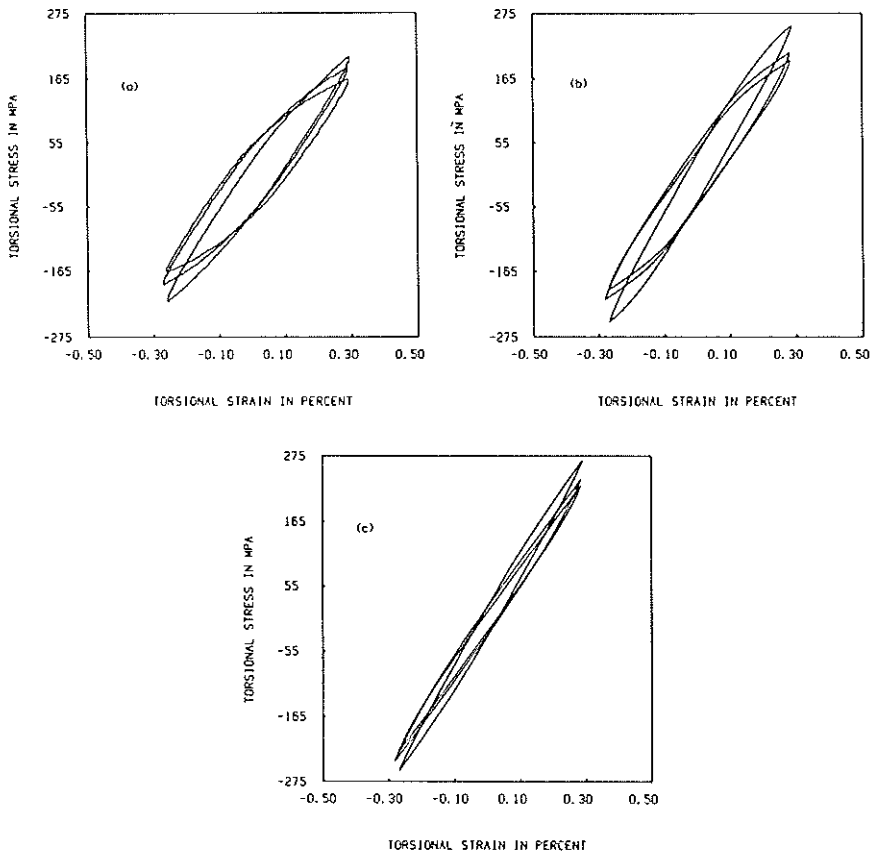

Fig 6 Steady state hysteresis loops at strain rates of 10^{-2}, 10^{-3}, and 10^{-5} per second in the [011] direction at 871°C (1600°F): (a) experimental; (b) theoretical predictions using octahedral and cube slip with the material constants in Table 3; (c) theoretical predictions using only octahedral slip

only by laborious slip trace studies that are very difficult to conduct at temperatures above 600°C (1100°F).

The material constants for the complete octahedral–cube slip model are given in Table 3 and were determined by correlating the [001] and [$\bar{1}$11] uniaxial hysteresis data in Figs 5(a) and 5(b). The torsional data in Fig. 6(b) is then a prediction. Alternatively, the uniaxial [001] data can be used to obtain the octahedral material constants and the cube constants may be determined by correlating the data in Fig. 6(b). The resulting [$\bar{1}$11] hysteresis loops may then be used to study the predictive capabilities of the formulation. Both methods have been tried and found satisfactory for determining the material constants in the model.

The material constants in the constitutive formulation were determined by

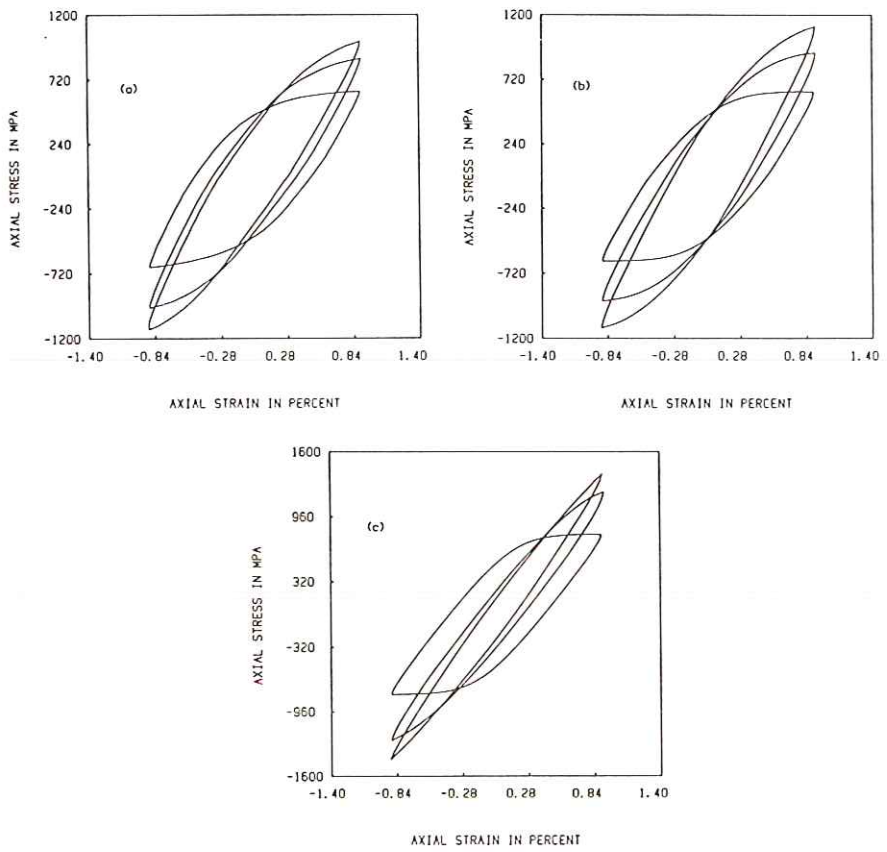

Fig 7 Steady state torsional hysteresis loops at strain rates of 10^{-3}, 10^{-4}, and 5×10^{-5} per second in the [001] direction at 871°C (1600°F): (a) experimental; (b) theoretical predictions using octahedral and cube slip with the material constants in Table 3; (c) theoretical predictions using only octahedral slip

applying optimization techniques to the problem. For this purpose a non-linear optimization code, CONMIN (**35**), was adapted for use on an IBM PC-XT. The Fortran optimization code can be interfaced with *any* constitutive integration subroutine through a user Fortran subroutine called ANALIZ. During the optimization process the main program calls subroutine ANALIZ to pass in the current values of the material constants and to calculate the objective function and constraints which are being minimized.

In subroutine ANALIZ a number of files containing the experimental data are read. Further calls to a subroutine which integrates the constitutive model over the strain histories corresponding to the experimental data files are then made, and the stresses computed with the constitutive model are compared with the stress values in the corresponding experimental data files. The

objective function, that is, the function being minimized, is computed by summing the square of the deviation between the computed and experimental stress values at a number of specified points of the loading history for each experimental data file of interest. In addition, constraints are applied to the problem, so that the error between the calculated and experimental stresses at specific data points is less than a prescribed amount (usually 1 per cent). The values of the objective function (constitutive error), the constraints, and the current values of the material constants are passed back to the main program by subroutine ANALIZ and the optimization code then determines a new set of material constants which gives a smaller value (less constitutive error) for the objective function. These new material constants are then passed back to subroutine ANALIZ and the process is repeated until the minimum objective function is found. At the objective minimum, the material constants will have their optimum 'non-linear least square' values.

The material constants presented in Table 3 were determined by optimizing the difference between the square of the experimental and theoretical values at various points on the steady state hysteresis loops. No 'errors' on the computer modelled 'non-linear least square' quantities are presented in Table 3. It is not

Table 3 Material constants for PWA 1480 at 871°C (1600°F)

$\alpha_{mm} = \alpha_{nn} = \alpha_{zz} = \alpha_{mz} = \alpha_{nz} = 0$	
$\varrho_1 = 6.06 \times 10^{11}$	N/m^2
$\varrho_2 = 7.95 \times 10^{6}$	
$\varrho_3 = 1.0 \times 10^{-12}$	$(N/m^2)^{-(m-1)} \cdot sec^{-1}$
$\varrho_4 = 0$	
$\varrho_5 = 0$	
$K_1 = 3.255 \times 10^{9}$	$N/m^2 \cdot sec^{(1/p)}$
$K_2 = 0$	$N/m^2 \cdot sec^{(1/p)}$
$m = 3.0$	
$p = 2.621$	
$s = 1$	
$\beta_1 = 0$	$N/m^2 \cdot sec^{(1/p)}$
$h_1 = 0$	$[N/m^2 \cdot sec^{(1/p)}]^{-(s-1)} \cdot sec^{-1}$
$\eta_1 = 0$	
$q = 1$	
$\varrho_6 = 1.593 \times 10^{11}$	N/m^2
$\varrho_7 = 9.41 \times 10^{6}$	
$\varrho_8 = 1.0 \times 10^{-12}$	$(N/m^2)^{-(n-1)} \cdot sec^{-1}$
$L_1 = 576.9 \times 10^{6}$	$N/m^2 \cdot sec^{(1/t)}$
$n = 3.0$	
$t = 8.63$	
$\beta_2 = 0$	$N/m^2 \cdot sec^{(1/t)}$
$\eta_2 = 0$	
$h_2 = 0$	$[N/m^2 \cdot sec^{(1/t)}]^{-(u-1)} \cdot sec^{-1}$
$u = 1$	
$D^c_{1111} = 213.2 \times 10^{9}$	N/m^2
$D^c_{1122} = 148.6 \times 10^{9}$	N/m^2
$D^c_{1212} = 100.0 \times 10^{9}$	N/m^2

appropriate to do so for highly nonlinear constitutive equations. For example, the asymptotic value of the stress at large strain values for uniaxial loading of a bar in the [001] orientation can be determined from Table 1. Since $\mathfrak{S} = 0$ (no cube slip), $\dot{c} = \dot{\varepsilon}$ (at large strain values the inelastic strain rate is approximately equal to the total strain rate), and $\omega = \varrho_1/\varrho_2$ at large strain rates where thermal recovery can be neglected, the third equation in Table 1 can be written in the form appropriate for monotonic loading of a uniaxial specimen with its axis in the [001] orientation as

$$\sigma = \varrho_1/(\varrho_2\mathfrak{D}) + (K/\mathfrak{D})(\dot{\varepsilon}/\mathfrak{B})^{(1/p)} \tag{30}$$

where $\mathfrak{B} = 8/\sqrt{6}$ and $\mathfrak{D} = 1/\sqrt{6}$. For a given strain rate, $\dot{\varepsilon}$, the value of $(\dot{\varepsilon}/\mathfrak{B})^{(1/p)}$ increases as the value of p increases. By decreasing the value of K as p is increased, the same asymptotic value of the stress in equation (30) can be maintained. It is, therefore, possible to model the stress–strain behaviour with widely varying values of K and p. Moreover, the asymptotic value of the equilibrium stress, ϱ_1/ϱ_2, can be changed as K and p change. The 'non-linear least square' values of the material constants are unique, but may be changed in concert within rather wide limits without significantly altering the calculated stress–strain curve.

The uniaxial relation for [001] orientated specimens given by equation (30) is useful in estimating the values of the octahedral material constants. In the case of $[\bar{1}11]$ orientated specimens, the cube slip component in the third equation of Table 1 is larger than the octahedral slip component. This can be seen by examining the width of the $[\bar{1}11]$ hysteresis loops when octahedral slip is assumed to be the only operative slip system in Fig. 5(c), compared with the width when cube slip is also assumed to be operative in Fig. 5(b). By ignoring the octahedral component in the third equation of Table 1, the corresponding expression for the stress at large strain values and at high strain rates (where thermal recovery is unimportant) for $[\bar{1}11]$ orientated specimens is given by

$$\sigma = \varrho_6/(\varrho_7\mathfrak{F}) + (L/\mathfrak{F})(\dot{\varepsilon}/\mathfrak{S})^{(1/n)} \tag{31}$$

where $\mathfrak{S} = \sqrt{2}$ and $\mathfrak{F} = 2/\sqrt{18}$. This expression is useful in estimating the cube material constants.

An examination of the material constant values given in Table 3 shows that many of the constants have been taken as zero. No non-Schmid terms have been allowed and the tensor α_{pq} has been set to zero. Again, at 871°C (1600°F), no cyclic hardening is observed in PWA 1480. The constants β_1 and β_2 which govern the rate at which the drag stresses in the octahedral and cube slip systems harden can therefore also be set to zero. This also applies to the dynamic and thermal recovery constants η_1, η_2, h_1, and h_2. The constants s and u have been set equal to unity since the values are immaterial when h_1 and h_2 are set to zero. In the same manner the constant q has been taken as unity since no latent hardening is observed in the single crystal material. However, if β_1 is taken as zero, the value of q is immaterial. It is seen that latent hardening has

been associated in the constitutive model with cyclic hardening, so that in the absence of cyclic hardening no latent hardening would be observed. At high temperatures most materials show little evidence of cyclic hardening and the current model would predict no latent hardening. Whether this is true for aluminium, copper, steel, Hastelloy-X, etc., is not known at present. However, for superalloys with the γ–γ' structure, little latent hardening is observed at any temperature.

Another interesting aspect of Table 3 is that the constants K_2, ϱ_4, and ϱ_5 have been set to zero. This implies that tension–compression asymmetry has been suppressed in the model at 871°C (1600°F). The reason for this is that experimental evidence shows that at temperatures below 871°C the tension–compression asymmetry can be predicted according to the cross-slip theory of Takeuchi and Kuramoto and by the Shockley partial constriction theory of Lall, Chin, Pope, Ezz, Paidar, Shah, and Duhl. However, at temperatures of 871°C (1600°F) and above, the preceding theories do not work. At lower temperatures the preceding theories are in accord with the experimental results in showing that the yield stress in tension exceeds that in compression in the [001] corner of the stereographic triangle, with the reverse being true in the [011] and [$\bar{1}$11] corners. At 871°C and above, the yield stress in compression exceeds that in tension in all three corners of the stereographic triangle at strain rates above 10^{-4} per second. The yield stress asymmetry also exhibits a strong strain rate dependence in which the yield stress is larger in tension than compression at low strain rates but is smaller in tension than compression at high strain rates. This dependence of the yield stress asymmetry on strain rate increases with temperature, and is evidently a diffusive mechanism which cannot be modelled at present. Until such a mechanism is introduced into the model it is necessary to set the asymmetry constants to zero at temperatures of 871°C (1600°F) and above in the current version of the constitutive formulation.

Conclusion

A slip system based constitutive model has been formulated for single crystal superalloys which represents, explicitly, both octahedral slip and cube slip. Tension–torsion tests on the single crystal alloy PWA 1480 have been run at 871°C (1600°F) and the torsional hysteresis loops, together with the prediction of the uniaxial hysteresis loops in crystallographic orientations corresponding to the three corners of the standard stereographic triangle, viz. [001], [011] and [$\bar{1}$11], have been successfully simulated using the single crystal model. It is found that the prediction of torsion data for a [001] orientated tubular specimen from [001] tension data, and the prediction of [011] and [$\bar{1}$11] axial data, is only successful if the correct combination of cube and octahedral slip is used. The prediction of torsion data is a useful tool in determining which slip modes are active.

Optimization techniques have proved to be a useful tool in determining the material constants for viscoplastic constitutive formulations. These techniques

can be used to determine the material constants for *any* constitutive model of interest.

Future work will involve simulations of various biaxial test conditions and will also attempt to simulate tests with variable strain rates and strain holds.

The single crystal constitutive model has been programmed as a Fortran subroutine and is now fully operational as part of the MARC, general purpose, non-linear finite element program.

Acknowledgements

The work reported herein was supported by the NASA Lewis Research Centre under grant NAG3-512 to the University of Connecticut. Helpful discussions with Dr R. Thompson, Dr R. Bill, and Dr G. Halford of the NASA Lewis Research Centre are acknowledged.

References

(1) McLEAN, M. (1983) *Directionally solidified materials for high temperature service*, The Metals Society, London.
(2) SABOL, G. P. and STICKLER, R. (1969) Microstructure of nickel-based superalloys, *Phys Stat. Sol.*, **35**, 11–52.
(3) POPE, D. P. and EZZ, S. S. (1984) Mechanical properties of Ni_3Al and nickel-base alloys with high volume fraction of γ', *Int. Met. Rev.*, **29**, 136–166.
(4) TAKEUCHI, S. and KURAMOTO, E. (1973) Temperature and orientation dependence of the yield stress in Ni_3Ga single crystals, *Acta Met.*, **21**, 415–425.
(5) LALL, C., CHIN, S., and POPE, D. (1979) The orientation and temperature dependence of the yield stress of $Ni_3(Al,Nb)$ single crystals, *Met. Trans.*, **10A**, 1323–1332.
(6) HIRTH, J. P. and LOTHE, J. (1982) *Theory of dislocations*, 2nd Edition, John Wiley, New York, p. 314.
(7) PAIDAR, V., POPE, D. P., and VITEK, V. (1984) A theory of the anomalous yield behavior in $L1_2$ ordered alloys, *Acta Met.*, **32**, 435–448.
(8) UMAKOSHI, Y., POPE, D. P., and VITEK, V. (1984) The asymmetry of the flow stress in $Ni_3(Al,Ta)$ single crystals, *Acta Met.*, **32**, 449–456.
(9) ESCAIG, B. (1968) Cross-slipping process in the F.C.C. structure, *Dislocation Dynamics*, Edited by ROSENFIELD, A. R., HAHN, G. T., BEMENT Jr, A. L., and JAFFE, R. I., McGraw-Hill, New York, pp. 655–677.
(10) SHAH, D. M. and DUHL, D. N. (1984) The effect of orientation, temperature and gamma prime size on the yield strength of a single crystal nickel-base superalloy, *Proc. 5th Int. Symp. on Superalloys*, ASM, Metals Park, Ohio, USA, pp. 105–114.
(11) GREENBERG, B. A., IVANOV, M. A., GORNOSTIREV, Yu. N., and KARKINA, L. E. (1978) Phenomenological theory of plastic deformation with several types of mobile and immobile dislocations, *Phys Stat. Sol. (a)*, **49**, 517–528.
(12) PASLAY, P. R., WELLS, C. H., and LEVERANT, G. R. (1970) An analysis of primary creep of nickel-base superalloy single crystals, *J. Appl. Mech.*, **37**, 759–764.
(13) PASLAY, P. R., WELLS, C. H., LEVERANT, G. R., and BURCK, L. H. (1971) Creep of single crystal nickel-base superalloy tubes under biaxial tension, *J. Appl. Mech.*, **38**, 623–626.
(14) BROWN, G. M. (1970) A self-consistent polycrystalline model for creep under combined stress states, *J. Mech. Phys Sol.*, **18**, 367–381.
(15) HUTCHINSON, J. W. (1976) Bounds and self-consistent estimates for creep of polycrystalline materials, *Proc. Roy. Soc. London*, **A348**, 101–127.
(16) WENG, G. J. (1983) The influence of fatigue stress on the creep behaviour of metals, *Acta Met.*, **31**, 207–212.
(17) WALKER, K. P. (1981) Research and development program for nonlinear structural

modelling with advanced time–temperature dependent constitutive relationships, NASA CR 165533, pp. 1–182.

(18) LINDHOLM, U. S., CHAN, K. S., BODNER, S. R., WEBER, R. M., WALKER, K. P., and CASSENTI, B. M. (1984) Constitutive modelling for isotropic materials (HOST), NASA CR 174718, pp. 1-1–A-68.

(19) LINDHOLM, U. S., CHAN, K. S., BODNER, S. R., WEBER, R. M., WALKER, K. P., and CASSENTI, B. M. (1985) Constitutive modelling for isotropic materials (HOST), NASA CR 174980, pp. 1–173.

(20) WALKER, K. P. and WILSON, D. A. (1984) Creep crack growth predictions in INCO 718 using a continuum damage model, NASA CP 2369, pp. 349–372.

(21) KAUFMAN, A., LAFLEN, J. H., and LINDHOLM, U. S. (1985) Unified constitutive models for nonlinear finite element structural analysis, NASA Technical Memorandum 86985 (presented at the 21st Joint Propulsion Conference, Monterey, California, USA, July 8–10), pp. 1–5.

(22) RAMASWAMY, V. G., VAN STONE, R. H., DAME, L. T., and LAFLEN, J. H. (1985) Constitutive modelling for isotropic materials (HOST), NASA CR 175004, pp. 1–233.

(23) ASARO, R. J. and RICE, J. R. (1977) Strain localization in ductile single crystals, *J. Mech. Phys Sol.*, **25**, 309–338.

(24) ASARO, R. J. (1983) Micromechanics of crystals and polycrystals, *Adv. Appl. Mech.*, **23**, 1–115.

(25) HUTCHINSON, J. W. (1970) Elastic–plastic behaviour of polycrystalline metals and composites, *Proc. Roy. Soc. London*, **A319**, 247–272.

(26) ASARO, R. J. (1979) Geometrical effects in the inhomogeneous deformation of ductile single crystals, *Acta Met.*, **27**, 445–453.

(27) PEIRCE, D., ASARO, R. J., and NEEDLEMAN, A. (1982) An analysis of nonuniform and localized deformation in ductile single crystals, *Acta Met.*, **30**, 1087–1119.

(28) HAVNER, K. S. (1981) Aspects of the simple theory of rotation-dependent crystal anisotropy, in *Plasticity of Metals at Finite Strain: Theory, Experiment, and Computation* (Proceedings of Research Workshop held at Stanford University, June 29–July 1, 1981), pp. 318–340.

(29) LEVERANT, G. R. and KEAR, B. H. (1969) The mechanism of creep in gamma prime precipitation-hardened nickel-base alloys at intermediate temperature, *Met. Trans*, **1**, 491–498.

(30) LEVERANT, G. R., KEAR, B. H., and OBLAK, J. M. (1972) Creep of precipitation-hardened nickel-base alloy single crystals at high temperature, *Met. Trans*, **4**, 355–362.

(31) KUJAWSKI, D. and KREMPL, E. (1981) The rate (time)-dependent behavior of Ti–7Al–2Cb–1Ta titanium alloy at room temperature under quasi-static monotonic and cyclic loading, *J. Appl. Mech.*, **48**, 55–63.

(32) OYTANA, C., DELOBELLE, P., and MERMET, A. (1982) Constitutive equations study in biaxial stress experiments, *J. Engng Mater. Technol.*, **104**, 1–11.

(33) LAMBA, H. S. and SIDEBOTTOM, O. M. (1978) Erasure of memory, and subsequent strain hardening, *J. Engng Mater. Technol.*, **100**, 98–103.

(34) McDOWELL, D. L. (1985) A two surface model for transient nonproportional cyclic plasticity: Part 1 – development of appropriate equations; Part 2 – Comparison of theory with experiments, *J. Appl. Mech.*, **52**, 298–308.

(35) VANDERPLAATS, G. N. (1973) *CONMIN – a Fortran program for constrained function minimization: User's manual*, NASA TMX-62282, pp. 1–60.